COBEM2015

ABCM Associação Brasileira de Engenharia e Ciências Mecânicas

23rd ABCM International Congress of Mechanical Engineering
December 6-11, 2015, Rio de Janeiro, RJ, Brazil

NUMERICAL PREDICTION OF THE NOISE GENERATED BY A REALISTIC LANDING GEAR

Paulo Rogério Gomes de Azevedo Junior
William Roberto Wolf
Universidade Estadual de Campinas, UNICAMP
paulo.statistician@gmail.com, wolf@fem.unicamp.br

Abstract. *The current paper presents noise predictions of the AIRBUS-ONERA LAGOON landing gear configuration. Numerical simulations of the turbulent flow past the LAGOON landing gear provide the acoustic sources responsible by the noise generation. The Ffowcs Williams & Hawkings (FWH) acoustic analogy formulation is then applied to perform the far-field noise predictions. Proper orthogonal decomposition is employed to extract the relevant noise sources from the turbulent flow and the noise predictions are accelerated by a 3D wideband fast multipole method. Therefore, a fast noise prediction framework is developed in the present work. Furthermore, a statistical treatment of noise sources and far-field noise is performed to correlate the effects of unsteady loads to noise radiation. Results are compared to experimental measurements and further numerical solutions available in the literature. An individual assessment of noise generation by the individual parts (wheels, strut, cavities and main axle) composing the landing gear is also presented.*

Keywords: *Landing gear noise, Aeroacoustics, Proper orthogonal decomposition*

1. INTRODUCTION

Noise regulations have become incrementally more stringent as air traffic has increased and will likely continue to do so in the future. In the last three decades, significant jet noise reduction has been achieved due to efforts on the design of more efficient and quieter engines. Since then, airframe noise associated with the unsteady turbulent flow around the aircraft has become a significant source of noise, specially for landing configurations (**?**). Therefore, improving prediction techniques for airframe noise generation and propagation is a key topic in aeroacoustics research.

The most significant airframe noise sources are high-lift components and landing gears. Recently, several efforts have been conducted in order to predict noise generation by landing gears and numerical and experimental studies were performed for simplified and realistic configurations (**??**). Currently, the American Institute of Aeronautics and Astronautics, AIAA, holds a workshop on benchmark problems for airframe noise computations, BANC, which fosters the discussion of relevant scientific and technological problems in airframe noise. Among the problems of interest lies the study of the LAGOON landing gear configuration which is analyzed here (**?**).

With current advances in computational power, turbulent flows over blunt bodies can be numerically resolved with significant accuracy. These unsteady flow simulations provide the noise sources which can then be used to predict the far-field noise. However, this hybrid numerical framework (computational fluid dynamics, CFD, + computational aeroacoustics, CAA) is still expensive since large computational grids and accurate algorithms are required to capture the most energetic flow scales in the numerical simulations. Furthermore, large datasets need to be computed and stored for the post-processing of the acoustic sources.

The current paper presents noise predictions of the AIRBUS-ONERA LAGOON landing gear configuration. Numerical simulations of the turbulent flow past the LAGOON landing gear provide the acoustic sources responsible by the noise generation. A simplified flow simulation dataset including only surface pressure is required for the far-field acoustic predictions which are performed using the Ffowcs Williams & Hawkings (FWH) acoustic analogy. Proper orthogonal decomposition is employed to extract the relevant noise sources from the turbulent pressure field and the noise predictions are accelerated by a 3D wideband fast multipole method. Therefore, a fast noise prediction framework is developed in the present work. With the present framework, reduced order models can be developed and applied for noise prediction by turbulent flows. A statistical treatment of the noise sources and far-field noise is performed to correlate the effects of unsteady loads to noise radiation. Results are compared to experimental measurements and further numerical solutions available in the literature (**?**). An individual assessment of the noise generation by the individual parts (wheels, strut, cavities and main axle) composing the landing gear is also presented.

2. FLOW SIMULATION AND ACOUSTIC PREDICTION

Compressible flow simulations of the LAGOON landing gear are performed using large eddy simulation. Since the interest here is to predict landing-gear far-field noise at landing and take off configurations, the flow is at a low Mach

number, $M_\infty = 0.18$. More details regarding the numerical methodology can be found in Ref. **?**. Results of the flow simulations are post-processed and the pressure signal is provided along the landing gear surface. After a statistical treatment this pressure signal is used as an input for the acoustic analogy formulation which provides the far-field noise.

The **?** (FWH) acoustic analogy formulation is used to predict the acoustic far-field noise radiated by the turbulent flow simulation. The FWH equation is applicable to bodies in arbitrary motion. However, in the present work, scattering bodies and observer locations are assumed to be in steady uniform motion in a stagnant medium. Following the development of **?**, the FWH formulation for steady uniform motion can be written as

$$\left[\hat{p'}H(f)\right] = -\int_{f=0}\left[i\omega\hat{Q}(\vec{y})G(\vec{x},\vec{y}) + \hat{F}_i(\vec{y})\frac{\partial G(\vec{x},\vec{y})}{\partial y_i}\right]dS - \int_{f>0}\hat{T}_{ij}H(f)\frac{\partial^2 G(\vec{x},\vec{y})}{\partial y_i \partial y_j}dV, \tag{1}$$

where p' is the pressure fluctuation, i is the imaginary unit, ω is the angular frequency, $f = 0$ represents the FWH surface and $H(f)$ is the Heaviside function defined as $H(f) = 1$ for $f > 0$ and $H(f) = 0$ for $f < 0$.

In the present work, the surface integrations appearing in Eq. 1 are computed along the landing gear surface, including wheels, cavities and axles. Therefore, the monopole source terms, $\hat{Q}$, become steady in time and do not appear in the frequency domain formulation. The dipole source terms, $\hat{F}_i$, are given by $\hat{F}_i = \hat{p'}\, n_i$ since, for the present high Reynolds number flow, viscous stresses are negligible. The term n_i appearing in the source term represents the component of the outward unit normal vector in the i Cartesian direction. The volume integrations of quadrupole sources in Eq. 1 are also neglected since, for low Mach number flows, the noise generated from quadrupole sources, $\hat{T}_{ij}$, are small compared to that radiated by dipole and monopole sources. For more details on the derivation of the source terms the authors refer the work by **?**.

In Eq. 1, the circumflex, $\hat{}$, denotes a frequency domain quantity. Considering a mean flow velocity in the x Cartesian direction, the 3D Green's function that incorporates convective effects (**?**) is given by

$$G(\vec{x},\vec{y}) = -\frac{e^{-ik\left[\sqrt{(x_1-y_1)^2+(1-M^2)[(x_2-y_2)^2+(x_3-y_3)^2]}-M(x_1-y_1)\right]/(1-M^2)}}{4\pi\sqrt{(x_1-y_1)^2+(1-M^2)\left[(x_2-y_2)^2+(x_3-y_3)^2\right]}}. \tag{2}$$

In Eq. 2, k is the wavenumber, M is the freestream Mach number defined as $M \equiv U_1/c_0$, $\vec{x} = (x_1, x_2, x_3)^t$ is an observer location and $\vec{y} = (y_1, y_2, y_3)^t$ is a source location.

In this work, the surface integrations of dipole source terms are performed using a 3D wideband multi-level adaptive fast multipole method (FMM) in order to accelerate the calculations. In the current context, the FMM consists of clustering noise sources from the landing gear CFD grid at different spatial lengths in multipole expansions and, then, evaluating their effects at clusters of observer locations well-separated from the noise sources. We define two well-separated clusters as sets of elements (sources and observers) that are circumscribed by spheres and whose centroids are distant from each other by a length of at least four times their radius.

In the FMM-FWH method, a cubical box surrounds a CFD grid containing noise sources and an acoustic grid containing many observer locations. Then, a recursive algorithm for the refinement of this box is applied in order to form the refinement levels of the multi-level FMM. The general idea consists of refining the box into eight smaller boxes and inspecting the number of sources and observers contained by each of the new boxes. This process continues until the number of elements inside all the boxes is smaller than or equal to a certain prescribed number. This prescribed number of elements per box will define the maximum refinement level in the FMM. Following an oct-tree algorithm, one can define sets of lists containing some specific boxes, such as boxes that share nodes or edges, well-separated boxes at the same level of refinement and others. These lists will help with the computation of multipole and local expansions including their translations and conversions. The authors refer the reader to the papers by **?** and **?** and the thesis by **?** for a complete description of the 3D wideband FMM.

3. Proper Orthogonal Decomposition

Proper Orthogonal Decomposition (POD) is a powerful method of data-analysis used to obtain a low-dimension approximation of a high-dimensional process; it is also known as Principal Component Analysis (PCA).

The POD technique provides a linear approximation of a set of functions that enable an easier characterization of the complex original input as a sum of weighted basis function. For practical applications, the decomposition can be carried out using the classical method or the snapshot method.

The fundamental idea of POD is to decompose a set of scalar quantity distributions $S^{(k)} = (S)^{(k)}_{(i,j)}$. Here, $S^{(k)}$ is the k snapshot of the S scalar quantity, for example, pressure or some component of velocity and the term i, j represents the index of the grid points where the scalar quantity distribution is obtained. The scalar field distribution is decomposed into a set of linear combinations of a M spatial basis functions (ϕ_m), and the corresponding temporal coefficients $c_m^{(k)}$, where

$$S^{(k)} = \sum_{m=1}^{M} c_m^{(k)}\phi_m$$

with the constraint that the basis function are orthonormal to each other.

The scalar quantities $S^{(k)}$ are reordered into a combination of rows and written in a matrix form as:

$$S = \begin{bmatrix} S^{(1)} \\ S^{(1)} \\ \vdots \\ S^{(K)} \end{bmatrix} = \begin{bmatrix} s^{(1)}_{i=1,j=1} & s^{(1)}_{i=1,j=2} & \cdots & s^{(1)}_{i=1,j=J} & s^{(1)}_{i=2,j=1} & \cdots & s^{(1)}_{i=I,j=J} \\ s^{(2)}_{i=1,j=1} & s^{(2)}_{i=1,j=2} & \cdots & s^{(2)}_{i=1,j=J} & s^{(2)}_{i=2,j=1} & \cdots & s^{(2)}_{i=I,j=J} \\ \vdots & \vdots & & \vdots & \vdots & & \vdots \\ s^{(K)}_{i=1,j=1} & s^{(K)}_{i=1,j=2} & \cdots & s^{(K)}_{i=1,j=J} & s^{(K)}_{i=2,j=1} & \cdots & s^{(K)}_{i=I,j=J} \end{bmatrix}.$$

Here, the terms I, J represent the total number of grid points in the x, y directions of the grid which describes the scalar field and K is the total number of snapshots. The spatial correlation matrix for the scalar field distribution is then defined by

$$C = \frac{1}{K}(SS^T).$$

The goal of using POD technique is to find a sequence of orthonormal basis functions representing the most 'coherent structures' in such a way that the following function is minimized

$$\sum_{k=1}^{K} \|S^{(k)} - \sum_{m=1}^{M} c_m^{(k)} \phi_m\|$$

subject to $(\phi_i, \phi_j) = \delta_{ij}$, where $\|.\|$ denotes the L^2 norm. This minimization is obtained solving the eigenvalue problem of correlation matrix C

$$C\beta_m = \lambda_m \beta_m.$$

In the present work, singular value decomposition is applied in order to obtain the eigenvalues.

4. RESULTS

The current section presents aeroacoustic results for the LAGOON landing gear configuration. Figure 1 shows the full geometry of the landing gear including its wheels, axle, cavities and strut (a), and detail views of the mesh along the wheels (b) and (c). Different sets of structured meshes are employed and the numerical CFD tool solves the compressible flow equations using an overset mesh approach. The total number of points along the surface of the landing gear is around 200000. In Fig. 2, one can see an exploded view of the individual parts of the landing gear.

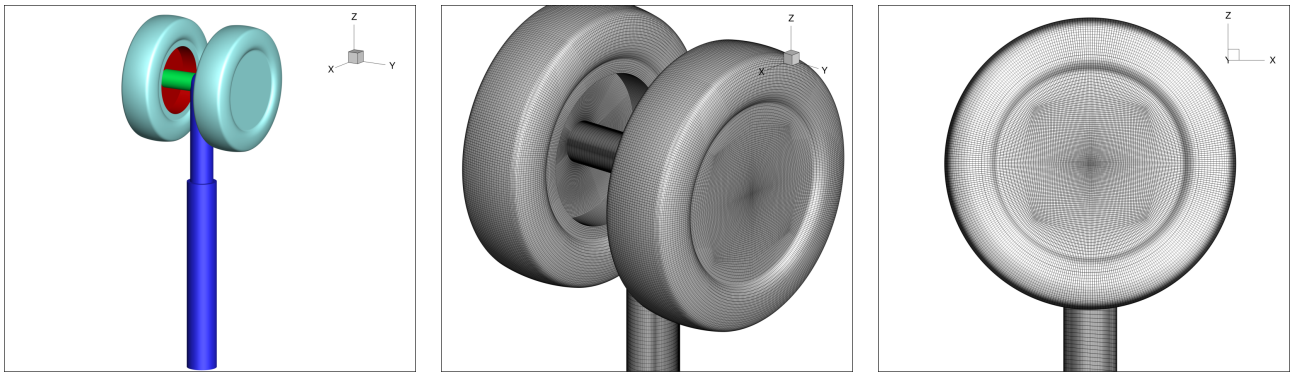

(a) Full view. (b) Mesh detail 1. (c) Mesh details 2.

Figure 1. LAGOON landing gear.

Figures 3 and 4 show the positions of far-field microphones and pressure probes along the wheels, respectively. Experiments and numerical simulations were conducted and data is provided in the literature for these microphone and probe locations. In this case, data is provided in terms of pressure spectra.

In Fig. 5, plots of power spectral density of surface pressure are shown for two near-field positions (probe locations K1 and K20 of Fig. 4). Results obtained by the present work are compared to data available in the literature. In the plots, the terms C19 and F2 represent experimental data from different wind tunnel test campaigns. The term ZDES represents data obtained from a detached numerical simulation, DES, also available in the literature. One can see that the comparison of PSD spectra between different experiments are similar as well as the comparison between the numerical simulations. However, the numerical simulations have a hard time resolving the small turbulent scales since DES and LES are employed. However, the low frequency content of the spectra show a good comparison. Figure 6 also presents plots of PSD, now measured at the far-field microphone locations M3, corresponding to sideline and flyover positions in Fig. 3.

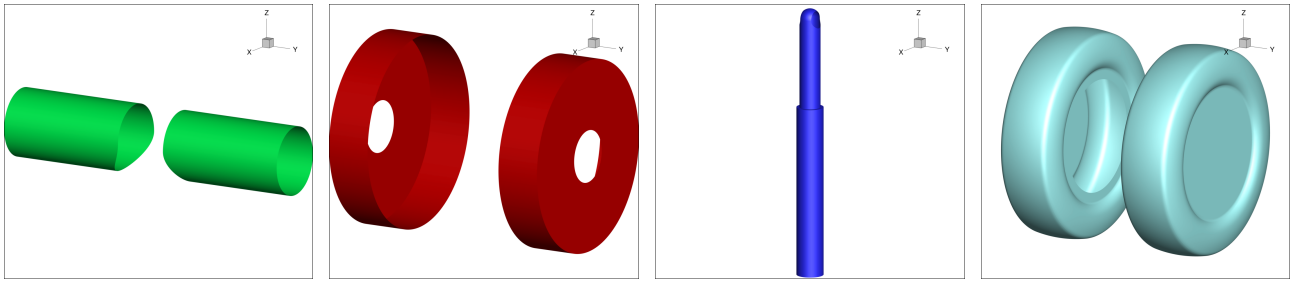

(a) Axle. (b) Rim. (c) Strut. (d) Wheels.

Figure 2. Exploded view of the landing gear.

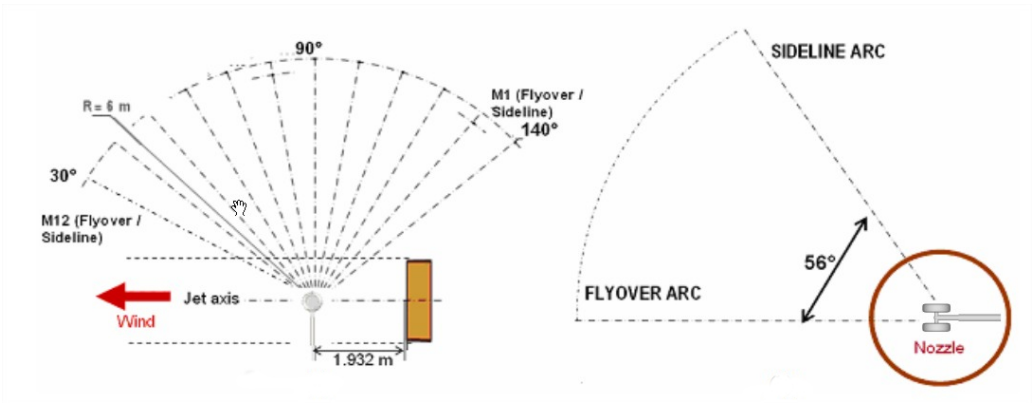

(a)

Figure 3. Far-field microphone locations where data is extracted in experiments and simulations.

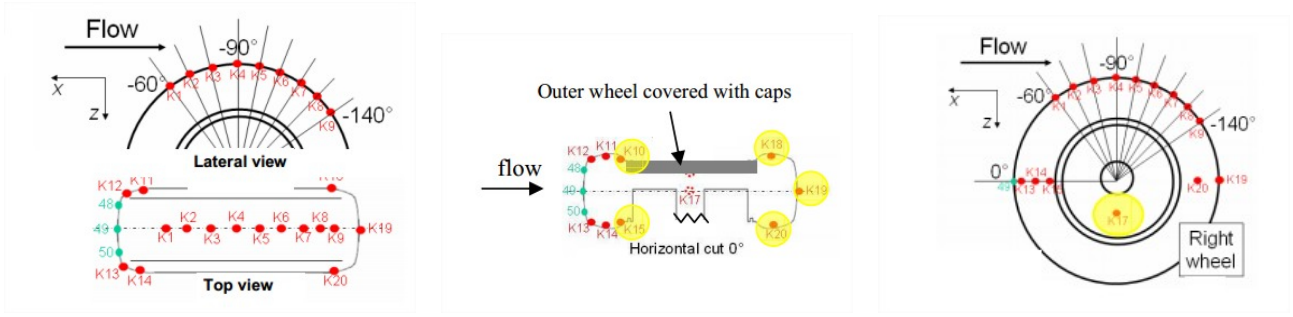

(a) (b) (c)

Figure 4. Surface pressure probe locations where data is extracted in experiments and simulations.

In this figure, it is possible to compare the far-field noise prediction from experiment and different numerical simulations. A good agreement is observed among all plots although the numerical predictions show closer match for all frequencies. Both the near and far-field pressure PSD plots shown are obtained after a statistical treatment of the CFD data. In this case, results of CFD are provided for each of the grid points composing the landing gear mesh. Time accuracy is enforced in the simulation and each grid point has a time signal with 20100 samples. This signal is split in bins with 50% overlap and spectra are computed by a fast Fourier transform of the windowed signals. The present plots show the results of the averaged spectra. For the far-field, the finite-difference grid is transformed in a finite volume grid with a connectivity table. Then, results of surface pressure are Fourier transformed and associated to each independent surface of the finite volume grid. Finally, the FWH equation is applied to radiate the far-field noise.

Once an excellent comparison is obtained between both CFD results, we want to perform an assessment of the individual noise sources in the landing gear. Therefore, the FWH equation is applied to the individual surfaces of the axle, wheels, rim and strut. Figure 7 shows the far-field PSD spectra obtained for each of these configurations. One can see that, at low frequencies, the axle and the rim are responsible for the major portion of the far-field noise radiation. Then, the noise from the wheels become relevant at around 1000 Hz. At high frequencies, the rims become, again, the major noise source.

Reduced-order modeling is an important tool which can be applied for the investigation of turbulent flows and aeroacoutics. In the present work, we apply POD to reconstruct the scattered pressure field along the landing gear surface and, then, we compute the far-field noise using the reconstructed pressure signal. In Fig. 8 (a), one can observe a plot showing

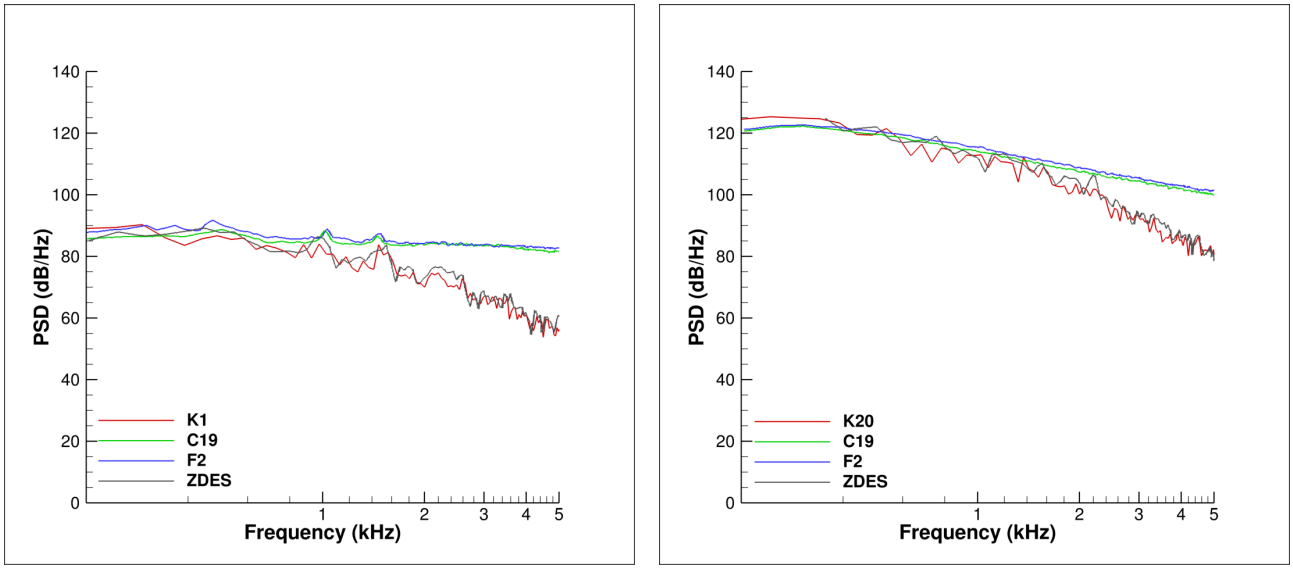

(a) Probe K1. (b) Probe K20.

Figure 5. Comparison of near-field results between experiments and numerical simulations.

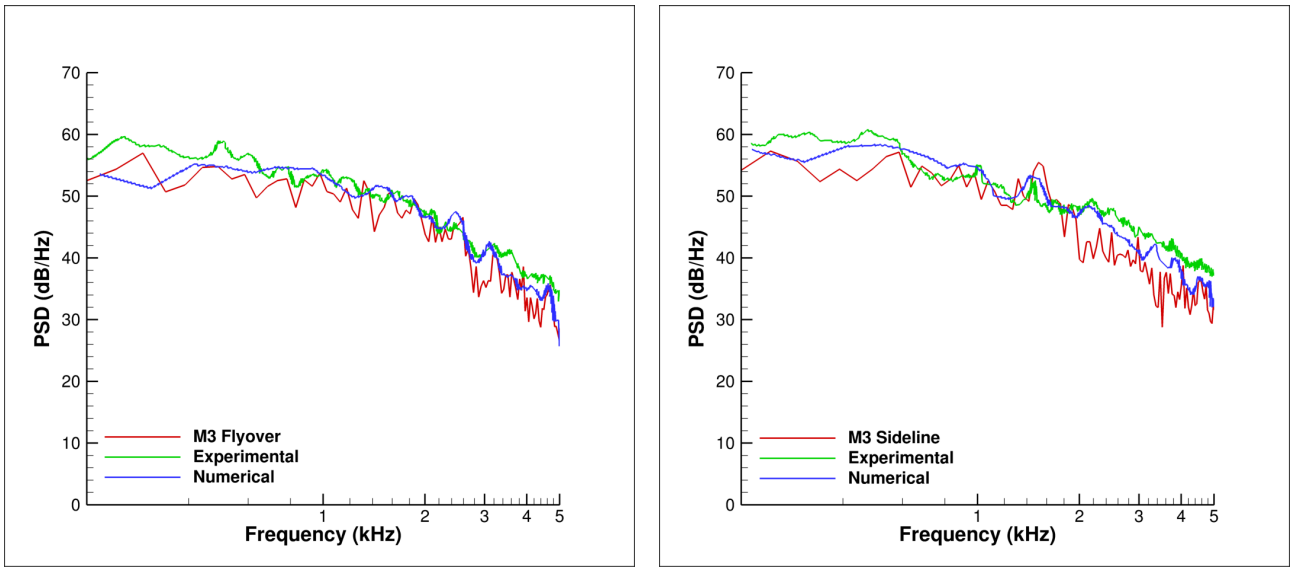

(a) Microphone M3 flyover. (b) Microphone M3 sideline.

Figure 6. Comparison of far-field results between experiments and numerical simulations.

the normalized modes of the present signal. Here, we are using the entire signal to perform POD, which means that 20100 modes build the complete signal. From the figure, it is possible to see that the first mode has 7% of the energy of the signal. Horizontal lines show the energy bands of the signal for 5%, 1% and 0.1% of the energy. In the plot, we see that the first 200 modes contain almost the entire energy of the signal. Figure 8 (b) shows the values of the correlation matrix, which is formed to resolve the POD of the system.

Different norms are employed for POD reconstruction of turbulent flows. If the flow is incompressible, a norm based on the kinetic energy is used to minimize the error. Different norms can be applied to compressible turbulent flows reconstructed using POD. The authors suggest the work from (**?**) for a discussion on the topic. In the present work, the POD reconstruction is implemented using the values of surface pressure only. Figure 9 presents the results of the POD reconstruction of the turbulent signal along the landing gear surface. One can observe that the pressure signal is recovered inside the rims using the first 30 modes. The strut signal is recovered using the first 60 modes. The small scale structures along the wheel surface are recovered using the first 150 modes.

Finally, Fig. 10 (a) shows the pressure signal after POD reconstruction. The signal is formed using the modes above 5%, 1% and 0.001% of the energy. This means that the first signal only has the first 2 modes, the second signal has the first 20 modes and the third signal is composed by the first 200 modes. The second signal is able to capture some of the large scale time fluctuations and the signal with 200 modes shows an excellent agreement with the original turbulent

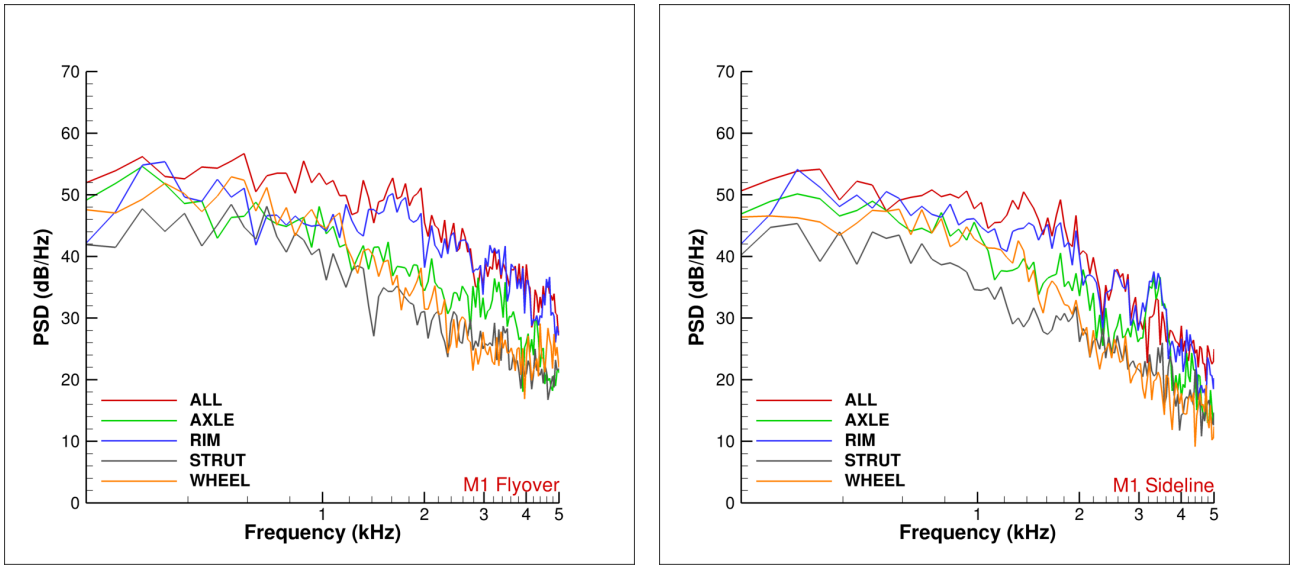

(a) Microphone M1 flyover.

(b) Microphone M1 sideline.

Figure 7. Comparison of the individual noise sources in the landing gear.

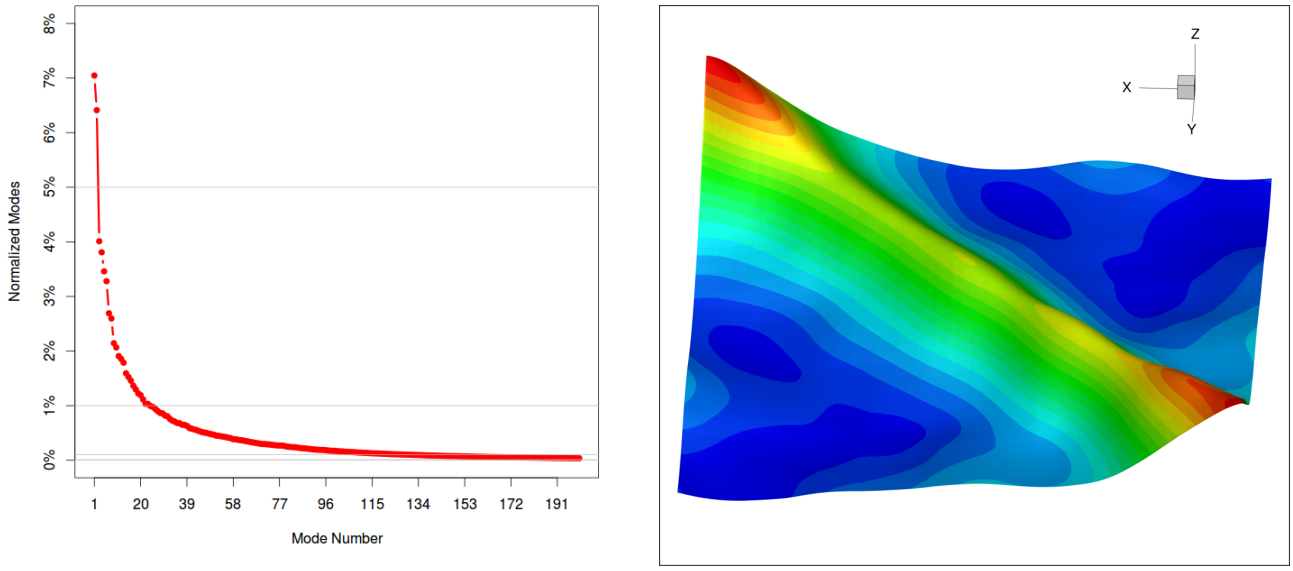

(a) Normalized modes.

(b) 3D visualization of the correlation matrix.

Figure 8. Application of POD to the pressure signal.

signal. The far-field spectra of the reconstructed signal for microphone M3 at flyover is shown in Fig. 10 (b). Using 200 modes, the far-field noise is predicted with accuracy, except for the high-frequency content, which depends on the capture of the fine turbulent scales.

5. CONCLUSIONS

The current paper presents noise predictions of the AIRBUS-ONERA LAGOON landing gear configuration. Acoustic predictions are obtained by the Ffowcs Williams & Hawkings acoustic analogy formulation. Results of far-field predictions are performed using the pressure fluctuations along the landing gear surface, obtained from compressible large eddy simulation. Proper orthogonal decomposition is also employed to reconstruct the turbulent signals and far-field predictions from the reconstructed signals show excellent agreement to those computed by the original signal.

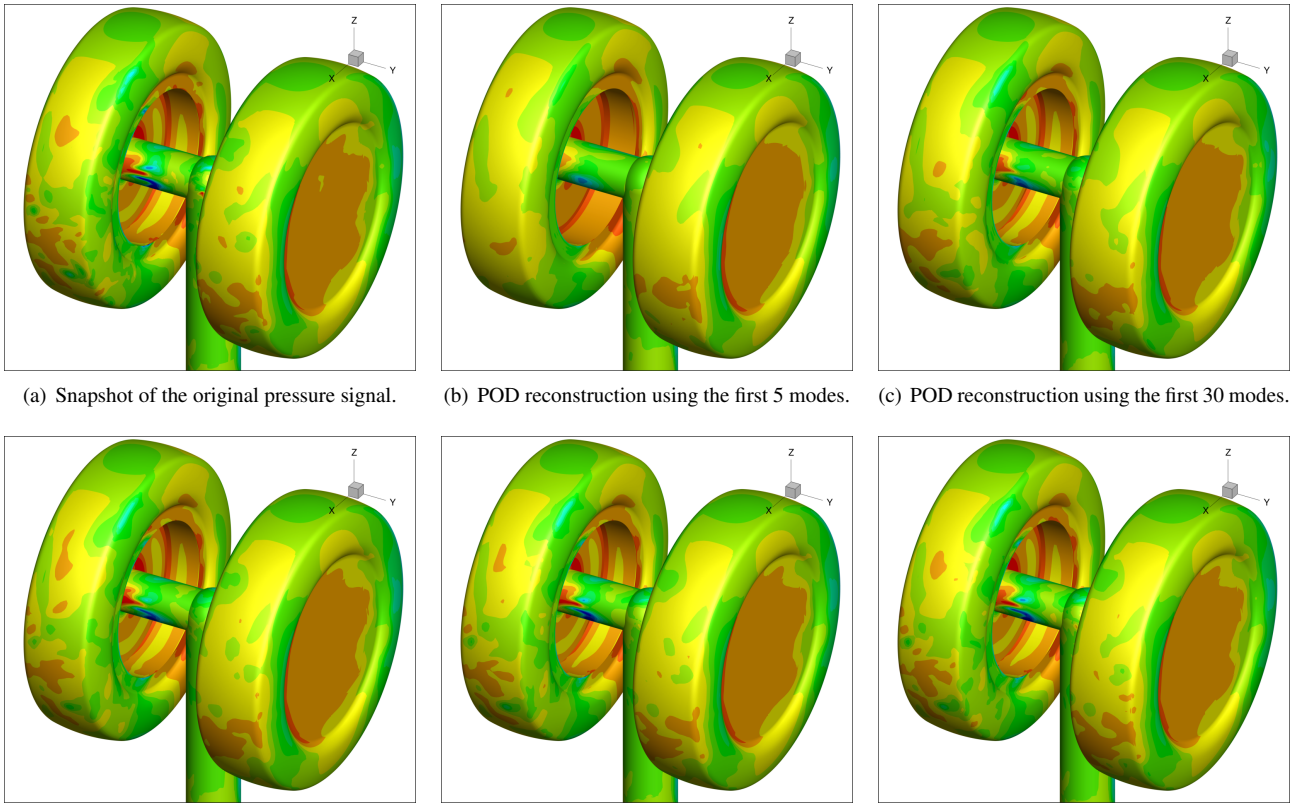

(a) Snapshot of the original pressure signal. (b) POD reconstruction using the first 5 modes. (c) POD reconstruction using the first 30 modes.

(d) POD reconstruction using the first 60 modes. (e) POD reconstruction using the first 90 modes. (f) POD reconstruction using the first 150 modes.

Figure 9. POD reconstruction of the turbulent signal.

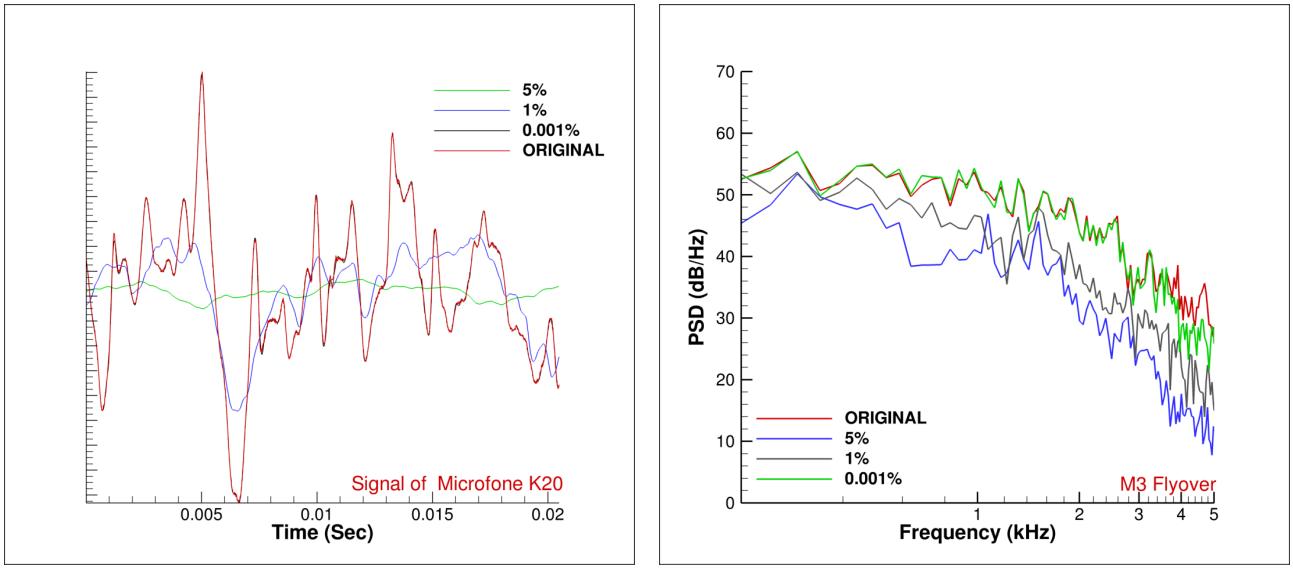

(a) Microphone K20 signal reconstruction using POD. (b) Far-field spectra of reconstructed signal for microphone M3 at flyover.

Figure 10. Exemplos POD

6. ACKNOWLEDGEMENTS

The authors acknowledge the financial support received from Fundação de Amparo à Pesquisa do Estado de São Paulo, FAPESP, under Grant No. 2013/03413-4 and from Conselho Nacional de Desenvolvimento Científico e Tecnológico, CNPq, under Grant No. 470695/2013-7. The authors also acknowledge FAPESP por providing a scholarship to the first author, Grant No. 2014/22202-7. The computational resources provided by CENAPAD-SP under Project No. 551 are also acknowledged.

7. REFERENCES

8. RESPONSIBILITY NOTICE

The following text, properly adapted to the number of authors, must be included in the last section of the paper: The author(s) is (are) the only responsible for the printed material included in this paper.